Clinical Radiology 74 (2019) 815.e15–815.e23

Contents lists available at ScienceDirect

Clinical Radiology

journal homepage: www.clinicalradiologyonline.net

Radiomics signature based on FDG-PET predicts proliferative activity in primary glioma

Z. Kong [a,b,1], J. Li [a,c,1], Zehua Liu [d,1], Zhenyu Liu [e,f], D. Zhao [g], X. Cheng [b], L. Li [d], Y. Lin [d,j], Y. Wang [a,*], J. Tian [e,f,h,i,**], W. Ma [a,***]

[a] *Department of Neurosurgery, Peking Union Medical College Hospital, Chinese Academy of Medical Sciences and Peking Union Medical College, Beijing, China*
[b] *Department of Nuclear Medicine, Peking Union Medical College Hospital, Chinese Academy of Medical Sciences and Peking Union Medical College, Beijing, China*
[c] *School of Medicine, Tsinghua University, Beijing, China*
[d] *Collaborative Innovation Center for Internet Healthcare, Zhengzhou University, Zhengzhou, Henan, China*
[e] *CAS Key Laboratory of Molecular Imaging, Institute of Automation, Chinese Academy of Science, Beijing, China*
[f] *University of Chinese Academy of Sciences, Beijing, China*
[g] *Department of Pathology, Peking Union Medical College Hospital, Chinese Academy of Medical Sciences and Peking Union Medical College, Beijing, China*
[h] *Beijing Advanced Innovation Center for Big Data-Based Precision Medicine, School of Medicine, Beihang University, Beijing, China*
[i] *Engineering Research Center of Molecular and Neuro Imaging of Ministry of Education, School of Life Science and Technology, Xidian University, Xi'an, Shaanxi, China*
[j] *School of Software, Zhengzhou University, Zhengzhou, Henan, China*

ARTICLE INFORMATION

Article history:
Received 25 February 2019
Accepted 26 June 2019

AIM: To investigate a radiomics method based on 2-[^{18}F]-fluoro-2-deoxy-D-glucose (FDG) positron-emission tomography (PET) to non-invasively evaluate proliferative activity in gliomas.

MATERIALS AND METHODS: A total of 123 patients with histopathologically confirmed primary glioma were reviewed retrospectively and assigned randomly into the primary cohort (n=82) and validation cohort (n=41). Tumour proliferative activity was defined by the Ki-67 index based on immunohistochemistry. Standard uptake value (SUV) maps were generated, and 1,561 radiomics features were extracted. Radiomics features were selected through the sequential application of three algorithms. Three predictive signatures were generated: a radiomics signature, a clinical signature, and a fusion signature. The predictive performances were evaluated by receiver operating characteristic (ROC) curve analysis, and patient prognoses were stratified based on the Ki-67 index and the signature with the most reliable performance.

* Guarantor and correspondent: Y. Wang, Department of Neurosurgery, Peking Union Medical College Hospital, Chinese Academy of Medical Sciences and Peking Union Medical College, Beijing, China. Tel.: +8615311860318.
** J. Tian, CAS Key Laboratory of Molecular Imaging, Institute of Automation, Chinese Academy of Science, Beijing, China. Tel.: +8601082618465.
*** W. Ma, Department of Neurosurgery, Peking Union Medical College Hospital, Chinese Academy of Medical Sciences, Peking Union Medical College, Beijing, China. Tel.: +8613701364566.
E-mail addresses: ywang@pumch.cn (Y. Wang), jie.tian@ia.ac.cn (J. Tian), mawb2001@hotmail.com (W. Ma).
[1] These authors contributed equally to this work.

https://doi.org/10.1016/j.crad.2019.06.019

RESULTS: Nine radiomics features were selected to construct the radiomics signature that achieved an accuracy of 81.7% and 73.2% and an area under the curve (AUC) of 0.88 and 0.76 in the primary cohort and the validation cohort, respectively. The clinical signature and fusion signature demonstrated comparable performance in the primary cohort but were over-fitted judging from the result in the validation cohort. Both the Ki-67 index and the radiomics signature could stratify patients into two distinctive prognostic groups, and the difference within each prognostic group was not statistically significant.

CONCLUSION: Radiomics signature based on ^{18}F-FDG-PET is a promising method for the non-invasive measurement of glioma proliferative activity and facilitates the prediction of patient prognoses.

Introduction

Glioma remains the most common malignant central nervous system (CNS) tumour for which treatment strategies and prognoses are determined based on the World Health Organization (WHO) grade, histopathological classification, and molecular information.[1,2] Tumour proliferative activity is usually measured by the expression of Ki-67, a protein encoded by the *MKI67* gene that serves as an element of the mitotic chromosomal periphery and prevents chromosomes from collapsing.[3] As Ki-67 is continuously expressed during the G1, S, G2, and M phases of mitosis,[4] immunostaining for Ki-67 is a reliable method to quantitatively assess the proliferative activity of tumours and has been widely used in the evaluation of gliomas. Furthermore, Ki-67 has been utilised in the assistance of tumour grading and found to be correlated with the prognosis of glioma patients[5–10]; however, the current measurement of tumour proliferative activity is predominantly determined by the immunohistochemistry of the Ki-67 protein based on tumour samples, which need to be collected at surgery or biopsy; thus, a non-invasive measurement of the Ki-67 index may have great influence for treatment planning and prognostic prediction.

Recent advances in radiomics have provide a powerful tool to explore the abundant information hidden in imaging data.[11] By extracting and selecting high-throughput radiomics features, tumour characteristics can be quantitatively depicted, and the specific tumour phenotype can be predicted by establishing a predictive mathematic model with selected relevant radiomics features.[12,13] In the field of glioma research, magnetic resonance imaging (MRI)-based radiomics has shown promising results in predicting the WHO grade, molecular characteristics, and patient prognoses.[14–20] In particular, Su *et al.* investigated the correlation between MRI radiomics features and Ki-67 expression levels in gliomas,[16] and Li *et al.* specifically focused on the prediction of Ki-67 expression in WHO grade II and grade III gliomas.[17]

2-[^{18}F]-fluoro-2-deoxy-D-glucose (FDG) positron-emission tomography (PET) is an established molecular imaging technique in which ^{18}F-FDG is taken up by the cells as glucose, but cannot be further catabolised, and its accumulation rate reflects the status of glucose metabolism.[21] ^{18}F-FDG-PET has been utilised in tumour grading, recurrence identification and prognosis prediction in the field of glioma research[22–24] and found to be somewhat correlated with Ki-67 expression levels in rat and human gliomas.[25,26] In addition, ^{18}F-FDG-PET based radiomics has been successfully utilised in multiple cancer types,[27–30] and alternative PET tracers have been developed as imaging markers of glioma proliferation[26]; however, to the authors' knowledge, no study has demonstrated the ^{18}F-FDG-PET characteristics of gliomas with different Ki-67 expression levels due to the standard uptake values (SUVs) and tumour-to-normal uptake ratios (TNRs), which are the most widely applied PET parameters but may not be capable of presenting features of the whole tumour.

This study retrospectively investigated the ^{18}F-FDG-PET imaging characteristics of gliomas using a radiomics approach, in order to build a reliable model to predict Ki-67 expression level and patients' prognosis non-invasively.

Material and methods

Patients

This study retrospectively evaluated 123 patients with histopathologically confirmed glioma. The inclusion criteria were as follows: (1) adults with histopathologically diagnosed primary WHO grade I–IV glioma from March 2010 to May 2018; (2) paraffin-embedded tumour tissue available for the measurement of the Ki-67 index; (3) preoperative ^{18}F-FDG-PET/CT examination with good imaging quality; (4) no anticancer therapies delivered before ^{18}F-FDG-PET/computed tomography (CT) examination or surgical operation; and (5) no previous history of CNS tumours. The study design and protocol were approved by the Institutional Review Board, and informed consent was obtained from all patients prospectively. The patients were randomly divided at a 2:1 ratio into a training cohort (n=82) and a validation cohort (n=41).

Ki-67 measurement

The Ki-67 index was determined by immunohistochemistry as described by Cai *et al.*[31] In short, formalin-fixed paraffin-embedded tumour tissues were sectioned

into 4-μm sections, after which the tissues were dewaxed and rehydrated. The inactivation of endogenous enzymes was performed with H_2O_2, and antigen recovery was completed with sodium citrate solution. After blocking the irrelevant antigens with bovine serum albumin, the sections were incubated with anti-human Ki-67 antibody (Abcam, UK) at 4°C overnight. The sections were subsequently incubated with an anti-rabbit antibody and diaminobenzidine (DAB) stained for the development of immunosignals, and finally stained with haematoxylin. Each section was reviewed by two neuropathologists with 11 and 16 years of clinical experience in neuro-oncology, and the percentage of cells expressing Ki-67 was calculated. Ki-67 was considered "low expression" if the positively stained cells were <10% and "high expression" if the positively stained cells were ≥10%.[31]

^{18}F-FDG-PET/CT data acquisition

Patients were required to fast for at least 4 hours before the ^{18}F-FDG-PET/CT examination, and blood glucose was confirmed to not exceed the normal limit (6.4 mM). ^{18}F-FDG, produced by an RDS-111 Cyclotron System (CTI, US), was administered at 5.55 MBq (0.15 mCi) per kilogram of body weight under standard conditions (quiet, dark room with patient's eyes closed). ^{18}F-FDG-PET/CT was performed on a Biograph 64 TruePoint TrueV PET/CT system (Siemens Medical Solutions, Germany) 40–60 minutes after the administration of ^{18}F-FDG, and 148 axial slides were acquired with an intersection space of 3 mm.

Image segmentation

Tumours were segmented by two experienced neurosurgeons who were blinded to the patient information, and a three-dimensional region of interest (ROI) was delineated on the ^{18}F-FDG-PET data using the ITK-SNAP software (http://www.itksnap.org/pmwiki/pmwiki.php). The two neurosurgeons had 14 and 29 years of clinical experience in neuro-oncology, and both of them had ≥10 years of experience in ^{18}F-FDG-PET. The ROI was then reviewed by a senior nuclear medical physician with 19 years of clinical experience in neuro-oncology. If the divergence of ROI by two neurosurgeons was <5%, the overlapping region was defined as the final ROI; and if the divergence was ≥5%, the senior nuclear medical scientist made the final decision.

Radiomics feature extraction

The SUV value of each pixel in the original ^{18}F-FDG-PET data was calculated with the following formula to generate an SUV map:

$$\mathrm{SUV} = \frac{Measure\ Activity_{(Bq/ml)}}{\frac{Injected\ Dose_{(mCi)}}{Decay\ Factor \times Body\ Weight_{(g)}}}$$

The decay factor was computed with the half-life of the tracer and time interval between the injection and collection. No further resampling was performed in order to preserve the original resolution.

A total of 1,561 radiomics features (including shape and size features, first-order features, texture features, wavelet features, and alternative filtered features) were extracted using PyRadiomics (https://github.com/Radiomics/pyradiomics),[32] and all radiomics features were subsequently normalised to a value between 0 and 1.

Radiomics feature selection and signature construction

Three steps of feature selection were sequentially utilised to reduce the complexity or bias of the radiomics feature set: Wilcoxon rank sum test was used to perform univariate analysis of feature differences between Ki-67 low expression and high expression cases in the primary cohort; multivariate linear logistic regression imposing L1 penalty on the regression coefficients was performed to further reduce the size of the feature set; and the final features were selected by a recursive feature elimination (RFE) algorithm with a fivefold cross-validation.[33] The radiomics signature was constructed with the selected radiomics features using a kernel-based support vector machine (SVM) on the primary cohort.[34,35]

Construction of the clinical and fusion signatures

Five clinical and clinically relevant imaging features, including age, sex, metabolic pattern (cystic or solid), maximum standard uptake value (SUVmax) and mean standard uptake value (SUVmean), were utilised to establish a clinical signature in the primary cohort using logistic regression after selection by the Akaike information criterion (AIC).[36,37] The five clinical features and selected radiomics features were combined and further selected by the AIC to generate the fusion signature.

Validation and evaluation of signatures

The signatures were validated on an independent validation cohort. Receiver operating characteristic (ROC) curves were generated, and the sensitivity, specificity, accuracy, positive predictive value, negative predictive value, and area under the curve (AUC) were calculated using both the primary cohort and the validation cohort to evaluate the performance of each radiomics signature. The Delong test was employed to measure the difference between signatures, and a decision curve analysis (DCA) was performed to demonstrate the clinical usefulness of the prediction models.

Prognostic analysis

The collection of survival data was terminated on 31 May 2018. Kaplan–Meier curves were generated based on the true Ki-67 index and the radiomics signature with best performance on the validation cohort to stratify patient prognoses. The log-rank test was performed to identify significant differences in survival between groups.

Statistical analysis

Statistical analysis was carried out using SPSS software, version 18.0 (SPSS, Chicago, USA) and R software, version 3.4.1, Vienna, Austria (www.R-project.org). Comparison between groups was undertaken using the independent sample *t*-test or Wilcoxon's rank sum test for quantitative variables and chi-square or Fisher's exact tests for categorical variables. Two-sided $p<0.05$ was considered statistically significant.

Results

Patient characteristics

The characteristics of the 123 included patients (82 patients in the primary cohort and 41 patients in the validation cohort) are demonstrated in Table 1. There were 54.9% (45/82) and 61% (25/41) cases displayed high Ki-67 expression level in the primary and validation cohorts, respectively. No significant interclass differences in age, sex, body weight, metabolic pattern, WHO grade, SUVmax, SUVmean were observed ($p=0.18-0.90$), and intraclass differences with the same trend in both cohorts existed regarding age, metabolic pattern, and WHO grade due to their correlation with Ki-67 expression.

Radiomics signature construction and validation

After the first step of feature selection, 1,071 of the 1,561 radiomics features remained, after which this number was reduced to 11 potential features with non-zero coefficients using a logistic regression model with L1 penalty. Finally, nine features were selected to construct the radiomics signature, and this signature achieved an AUC of 0.88 and an accuracy of 81.7% for predicting Ki-67 expression levels in the primary cohort. The radiomics signature was further verified in the validation cohort and displayed an AUC of 0.76 and an accuracy of 73.2%. The selected radiomics features are detailed in Table 2. The predictive performance of the radiomics signature is shown in Table 3. The ROC curve and bar plot of the radiomics signature are displayed in Fig 1.

Performance of clinical and fusion signatures

Sex and metabolic patterns were selected by AIC from the five clinical features to build the clinical signature, and reached an AUC of 0.84 and an accuracy of 75.6% in the primary cohort; however, the performance of the clinical signature decreased to an AUC of 0.67 and an accuracy of 65.9% in the validation cohort. Sex, metabolic patterns, SUVmean, together with the nine selected radiomics features were selected by AIC to build the fusion signature, and demonstrated AUCs of 0.92 and 0.73, accuracies of 81.7% and 78% in the primary and validation cohorts, respectively. The Delong test showed a significantly better performance of the fusion signature than the radiomics signature and clinical signature ($p=0.048$ and 0.015, respectively) in the primary cohort, and the differences between signatures in the validation cohort did not reached statistically significance ($p=0.082-0.689$). The performances of the clinical and fusion signatures are displayed in Table 3. The ROC curves of the two signatures are displayed in Fig 1.

Table 2
Selected features in the radiomics signature.

Feature Name	Matrix	Filter
Median	First order	Local binary patterns-3D-ml
Difference variance	GLCM	Logarithm
Run entropy	GLRLM	Gradient
Skewness	First order	Wavelet-HLH
Correlation	GLCM	Wavelet-HLL
Small dependence high grey-level emphasis	GLDM	Logarithm
Difference variance	GLCM	Square root
Range	First order	Wavelet-HHH
Small area low grey-level emphasis	GLSZM	Local binary patternsc-3D-k

GLCM, grey-level co-occurrence matrix; GLRLM, grey-level run length matrix; GLSZM, grey-level size zone matrix; GLDM, grey-level dependence matrix; 3D, three-dimensional.

Table 1
Patients' characteristics of primary and validation cohorts.

Characteristics	Primary cohort ($n=82$)			Validation cohort ($n=41$)			*p*-Value
	≥10% ($n=45$)	<10% ($n=37$)	*p*-Value	≥10% ($n=25$)	<10% ($n=16$)	*p*-Value	
Age (mean ± SD, years)	51.51±14.89	40.86±14.30	0.002	48.24±13.20	46.94±14.51	0.77	0.72
Sex			0.15			0.12	0.90
Male	29	18		17	7		
Female	16	19		8	9		
Metabolic pattern			<0.001			0.19	0.18
Cystic	20	36		12	11		
Solid	25	1		13	5		
WHO grading			<0.001			<0.001	0.69
Low-grade glioma	4	24		3	13		
High-grade glioma	40	13		22	3		
SUVmax	10.80±6.16	9.57±4.65	0.09	11.34±5.40	8.92±2.12	0.19	0.40
SUVmean	4.55±2.34	4.19±1.75	0.25	4.95±2.13	4.25±1.09	0.36	0.20

Chi-square or Fisher's exact tests, as appropriate, were used to compare the differences in categorical variables; the independent sample t-test was used to compare the differences in age; the Wilcoxon rank sum test was used to compare the difference in SUVmax and SUVmean.
SD, standard deviation; WHO, World Health Organization; SUV, standard uptake value.

Table 3
The performances of the three predictive models.

Models		AUC (95%CI)	ACC	SEN	SPE	PPV	NPV
Radiomics model	Primary cohort	0.88 (86.2,90.5)	81.7%	95.6%	64.9%	76.8%	92.3%
	Validation cohort	0.76 (72.6,78.9)	73.2%	92%	43.8%	71.9%	77.8%
Clinical model	Primary cohort	0.84 (82,86.6)	75.6%	57.8%	97.3%	96.3%	65.5%
	Validation cohort	0.67 (62.7,70.1)	65.9%	72%	56.3%	72%	56.3%
Fusion model	Primary cohort	0.92 (91,94)	81.7%	84.4%	78.4%	82.6%	80.5%
	Validation cohort	0.73 (69.3,76.7)	78%	84%	68.8%	80.8%	73.3%

CI, confidence interval; AUC, area under receiver-operating characteristic curve; ACC, accuracy predictive value; SEN, sensitivity; SPE, specificity; PPV, positive predictive value, NPV, negative predictive value.

The decision curve that demonstrated the patients benefit using the radiomics signature showed a net benefit over both schemes if the threshold probability was >10% in the primary cohort and >30% in the validation cohort. The decision curves in the primary and validation cohort are displayed in Fig 2a and b. Examples of the radiomics signature that predicts Ki-67 expression level under similar clinical features and ^{18}F-FDG-PET images are shown in Fig 3.

Prognostic prediction

One-hundred and seventeen of the 123 patients for whom the exact time of death was available or who were known to survive before the closing date were included in the prognostic analysis. Both the Ki-67 expression level and the radiomics signature could stratify glioma patients into a long-survival group and a short-survival group ($p \leq 0.01$), and the difference between groups did not reach statistical significance. The Kaplan–Meier curves are displayed in Fig 2c.

Discussion

In this study, Ki-67 expression level related ^{18}F-FDG-PET radiomics features were selected and analysed, and a radiomics signature, a clinical signature, and a fusion signature that combined radiomics and clinical features were constructed to determine the proliferative activity of gliomas. The radiomics signature demonstrated a stable and reliable performance, reaching an accuracy of 81.7% and 73.2% and an AUC of 0.88 and 0.76 in the primary and validation cohorts, respectively, suggesting the reliability of ^{18}F-FDG-PET-based radiomics to non-invasively predict Ki-67 expression in gliomas. Furthermore, both the Ki-67 index and radiomics signature stratified the patients into two distinct prognostic groups, indicating the clinical value of the prediction model.

Previous studies on the non-invasive surrogate measurement of Ki-67 in gliomas were predominately based on quantitative parameters or radiomics features of conventional or advanced MRI series,[16,17,38–40] and the predictive performance of these models (if reported, without distinction between the training result and validation result, because not all studies have a validation cohort) showed an accuracy ranging from 0.76–0.88, while the AUC ranged from 0.78–0.93. The radiomics signature in the present study showed a comparable accuracy and AUC value, demonstrating the competency of predicting proliferative activity through ^{18}F-FDG-PET-based radiomics features. The non-invasive measurement of tumour aggressiveness and invasiveness is crucial not only for determining the duration of tumorigenesis but also for predicting tumour behaviour and guiding therapeutic strategies (e.g., time and extent of surgery) and for making the most appropriate treatment decisions. Although there may be differences in imaging characteristics among tumours with different WHO grades and pathological subtypes, the present radiomics signature has shown the ability to predict tumour proliferative activity without invasive information, thereby demonstrating the generalisability of the prediction model. Nevertheless, Ki-67 is a semi-quantitative marker for proliferation activity and often encounters intra-observer and interobserver divergences.[41] Although two neuropathologists separately reviewed the Ki-67 index in the present study, in 4.1% (5/123) patients they did not reach agreement in the initial classification and these patients were re-evaluated. Therefore, the radiomics signature that predicts Ki-67 level may not completely reflect the proliferation activity of gliomas.

In comparison with structural imaging methods such as CT and MRI, PET is an alternative imaging technique that measures tumour metabolism with a low concentration of radiolabelled substrate. As tumours often exhibit altered glucose metabolism (also known as the Warburg effect,[42,43] in which cancer cells produce energy through glycolysis followed by lactic acid fermentation instead of oxidative phosphorylation), glucose analogues (e.g., ^{18}F-FDG) have become the most common radiotracers in cancer evaluation[44]; however, as shown in Table 1, Ki-67 expression demonstrates only moderate correlation with conventional quantitative parameters of ^{18}F-FDG-PET.[45] Considering the regulation of glucose metabolism by several oncogenic pathways (e.g., the PI3K/AKT/mTOR pathway, the p53 pathway),[44] there is strong potential to evaluate the proliferative activity of gliomas using a radiogenomic approach. To the authors' knowledge, the present study is the first to explore the proliferation status of gliomas based on ^{18}F-FDG-PET data using a radiomics approach and yield acceptable results, suggesting the reliability of the theory and techniques. In addition, the reconstruction technique of PET images is different from that of MRI images, which leads to a relatively lower spatial resolution of ^{18}F-FDG-PET than that of structural images and may influence the stability of

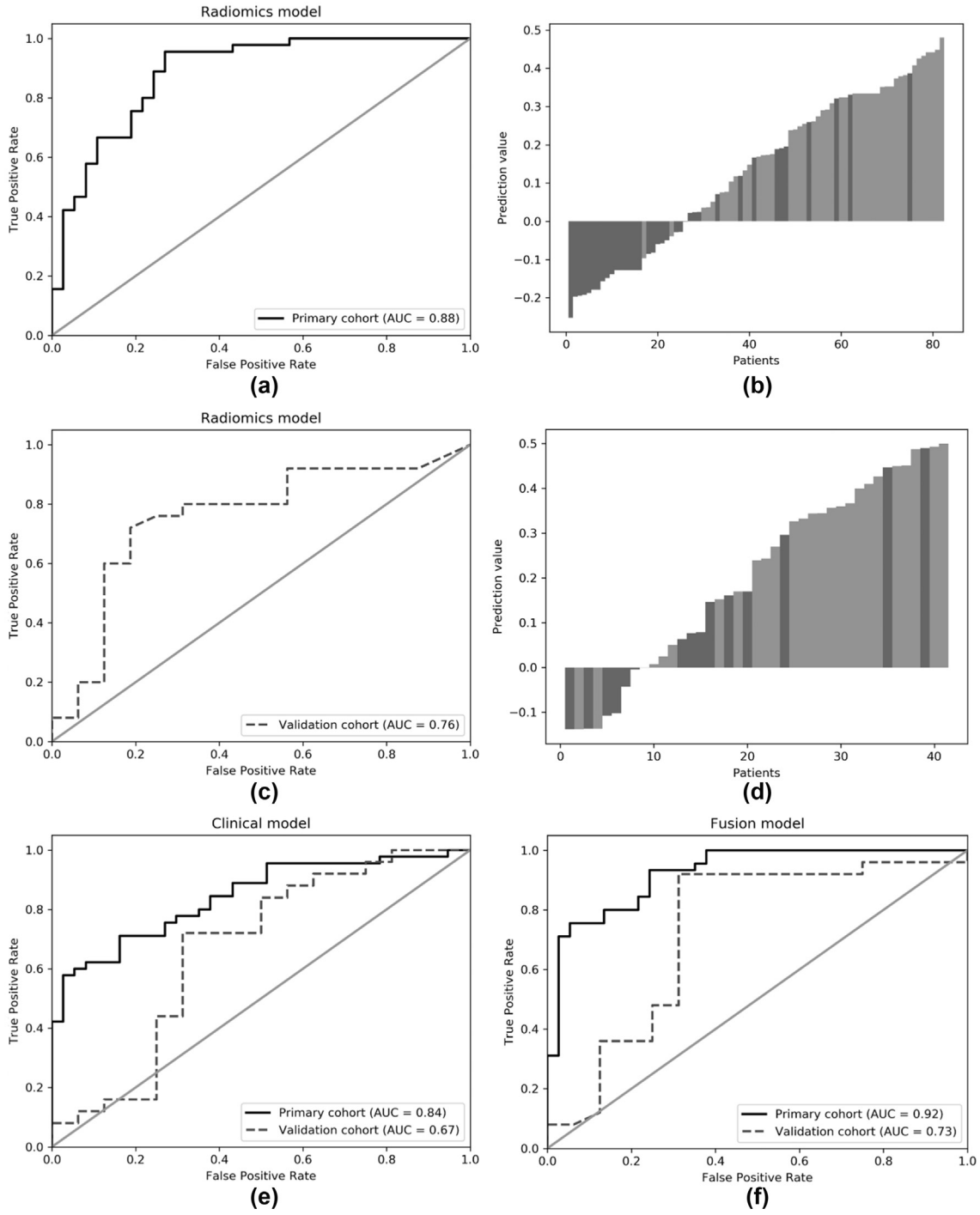

Figure 1 Performance of the three predictive signatures. The predictive performance of the radiomics signature in the primary cohort was evaluated by a ROC curve (a) and bar plot (b). The light bars with predictive value >0 and the dark bars with the predictive value <0 indicate an accurate classification by the radiomics signature. (c,d) The performance of the radiomics signature was also evaluated in the validation cohort. The ROC curves of the clinical signature (e) and fusion signature (f) in the primary and validation cohorts are also displayed.

certain radiomics features. Thus, the selection of appropriate radiomics features has become a key step in PET radiomics studies.

In this study, three algorithms were utilised sequentially to reduce redundant features and select appropriate features for the construction of the radiomics signature. The exclusion of irrelevant features is crucial because these features may conceal the value of relevant features and affect the performance of the prediction model; however, 68.6% of the features remained after the Wilcoxon rank sum test, suggesting that most ^{18}F-FDG-PET-based radiomics features are relevant to the proliferative activity of the tumour. Features were further reduced to obtain a feasible number with a balance between under-fitting and over-

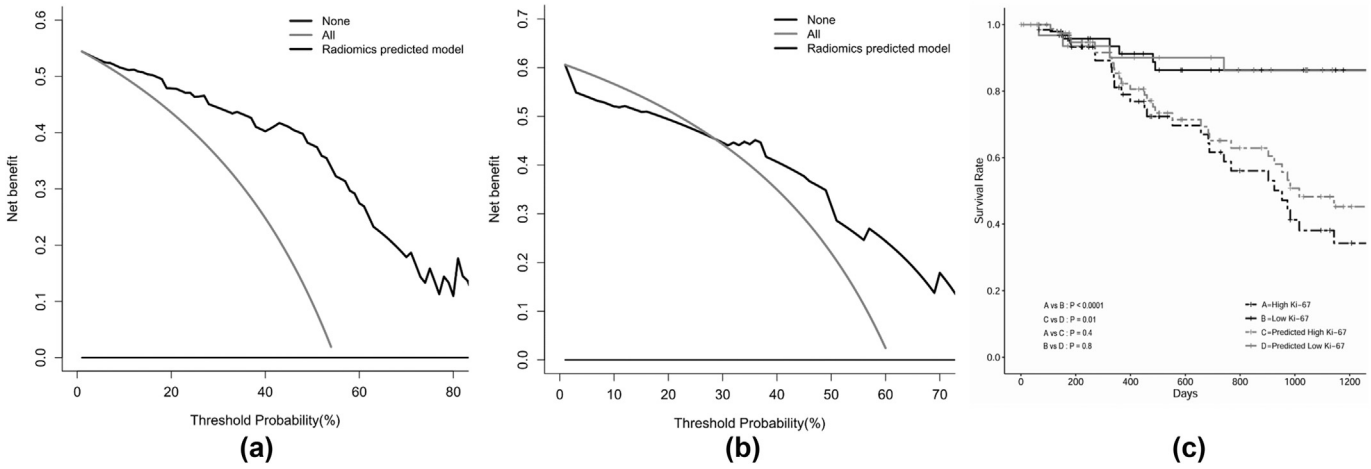

Figure 2 Clinical value of the radiomics signature. The decision curve of the radiomics signature demonstrates the benefit to the patients in the primary cohort (a) and validation cohort (b). (c) Kaplan–Meier curves display the stratification of prognosis by the Ki-67 index and radiomics signature.

fitting. As radiomics studies extract numerous features in a relatively limited cohort, the inclusion of excessive features in the prediction model may increase performance in the primary cohort, but decrease it in the validation cohort and further lower the generalisability of the model.

Patient sex and the metabolic pattern (cystic or solid) were selected by the AIC to build the clinical signature, but patient age and the frequently used quantitative parameters (e.g., SUVmax, SUVmean) were excluded because they cannot significantly contribute to the prediction model. Although the clinical signature revealed a similar AUC in the primary cohort to the radiomics model, the AUC of the clinical signature in the validation cohort decreased by 0.17 compared with than in the primary cohort, suggesting that overfitting had occurred in the clinical model. Although the combination of clinical features and radiomics features demonstrated a significantly better performance than the radiomics model in the primary cohort, the fusion model may also be over-fitted judging from the AUC value of the validation cohort. Thus, although clinical features may be relevant with tumour proliferative activity, the radiomics signature remains the most stable and should be utilised as a non-invasive tool to evaluate tumour proliferative activity as well as patient prognosis. Although most selected radiomics features underwent filtering, and therefore, were not visually recognisable for physicians, the radiomics approach did stratify patients into a high proliferative group and a low proliferative group, thereby aiding nuclear medical physician to non-invasively determine tumour proliferation activity (Fig 3).

The prognostic value of Ki-67 in gliomas has been investigated previously in several retrospective studies,[5–8,10] and a

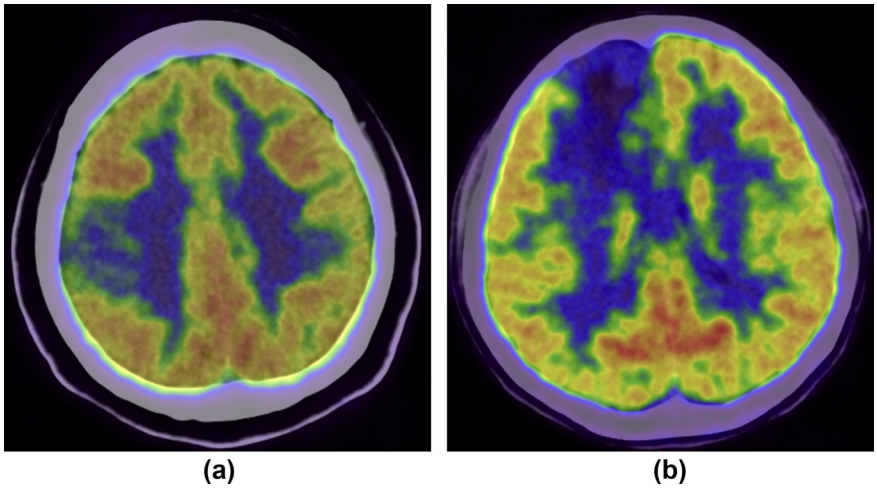

Figure 3 Examples of radiomics signature that predict tumour proliferative activity. (a)A 56-year-old female patient with histopathological diagnosed WHO grade II astrocytoma (Ki-67 index = 23%), and (b) a 37-year-old female patient with histopathological diagnosed WHO grade II astrocytoma (Ki-67 index = 8%). The determination of tumour proliferative activity is difficult based on clinical features; however, the radiomics signature demonstrated the values of 0.67 (a) and 0.27 (b) in these two patients, which successfully stratified the patients into the high proliferative activity group and low proliferative activity group (cut-off value = 0.39).

meta-analysis that included 4,307 glioma patients from 51 studies demonstrated a correlation of high Ki-67 expression with poor overall survival (OS, hazard ratio [HR] = 1.66) and poor progression-free survival (PFS, HR = 1.67)[9]. The results of the present were consistent with previous findings, in which the Ki-67 expression level stratified glioma patients into two significantly different groups based on prognosis ($p<0.0001$). Radiomics signatures would provide substantial value if they predict not only the proliferative activity of tumours but also the prognosis of patients. In the present study, the radiomics signature could stratify patients into two distinct prognostic groups ($p=0.01$), indicating the ability of the signature to predict prognosis before surgery or therapy. Although there was a difference in population between the prognostic groups stratified by the Ki-67 index and the radiomics signature, the results of log-rank tests demonstrated no significant difference within each group (e.g., the Kaplan–Meier curves of the long-survival group identified by the Ki-67 index and radiomics signature almost coincided, and the difference was non-significant), suggesting the accuracy of the prognostic prediction by the radiomics signature. Nevertheless, many patients did not meet the endpoint during the collection of prognostic data, which may have led to bias in the stratification of prognosis.

The current study has several limitations. First, this was a retrospective study based on a relatively small number of patients from a single centre, and this may have resulted in bias regarding patient selection and thus prevents the generalisation of the prediction model. The ^{18}F-FDG-PET images were acquired on a single PET system, and scanner or scan protocol-related factors may have influenced the stability of the radiomics signature. Further large-scale prospective studies with multicentre data may be necessary to improve the performance and generalisability of the prediction model. Second, only the tumour region, but not the surrounding oedema was segmented, and this may have resulted in the loss of certain features of proliferation because glioma grows in an infiltrative manner. Third, the Ki-67 index may not be calculated from the ^{18}F-FDG avid areas, and further biopsy-guided regional image studies may better reflect and predict the local proliferative activity of gliomas.[46] Fourth, the prognostic analysis was carried out without knowledge of treatment strategies (e.g., excision extent, chemotherapy regimen, radiotherapy dose), so some influencing factors could not be excluded. More comprehensive data regarding treatment and progression-free survival could thus be integrated. Finally, only ^{18}F-FDG-PET images were utilised in this radiomics study. Alternative amino acid- or choline-based PET images and multimodal imaging data (e.g., MRI) could be further integrated into the prediction of glioma proliferation.

In conclusion, radiomics signature based on ^{18}F-FDG-PET is a promising tool, similar to MRI radiomics, for the non-invasive detection of glioma proliferative activity and can facilitate prognostic prediction in glioma patients before the delivery of therapies. Further large-scale prospective radiomics studies with multimodal imaging data could promote the prediction performance as well as the clinical translation of the study results.

Conflict of interest

The authors declare no conflict of interest.

Acknowledgements

This work was supported by the Chinese Academy of Medical Sciences which funded the Chinese Academy of Medical Sciences Innovation Fund for Medical Sciences (grant numbers 2016-I2M-2-001, 2018-I2M-3-001), the Fundamental Research Funds for the Central Universities (grant number 3332018029), the National Natural Science Foundation of China (grant numbers 81772009, 81772012), the Scientific and Technological Research Project of Henan Province (grant number 182102310162), the Beijing Natural Science Foundation (grant number 7182109), and the Chinese Academy of Sciences (grant numbers GJJSTD20170004 and QYZDJ-SSW-JSC005). The authors thank American Journal Experts for providing language help.

References

1. Lapointe S, Perry A, Butowski NA. Primary brain tumours in adults. *Lancet* 2018;**392**(10145):432–46.
2. Jiang T, Mao Y, Ma W, *et al*. CGCG clinical practice guidelines for the management of adult diffuse gliomas. *Cancer Lett* 2016;**375**(2):263–73.
3. Cuylen S, Blaukopf C, Politi AZ, *et al*. Ki-67 acts as a biological surfactant to disperse mitotic chromosomes. *Nature* 2016;**535**(7611):308–12.
4. Gerdes J, Lemke H, Baisch H, *et al*. Cell cycle analysis of a cell proliferation-associated human nuclear antigen defined by the monoclonal antibody Ki-67. *J Immunol* 1984;**133**(4):1710–5.
5. Wakimoto H, Aoyagi M, Nakayama T, *et al*. Prognostic significance of Ki-67 labeling indices obtained using MIB-1 monoclonal antibody in patients with supratentorial astrocytomas. *Cancer* 1996;**77**(2):373–80.
6. Neder L, Colli BO, Machado HR, *et al*. MIB-1 labeling index in astrocytic tumours—a clinicopathologic study. *Clin Neuropathol* 2004;**23**(6):262–70.
7. Johannessen AL, Torp SH. The clinical value of Ki-67/MIB-1 labeling index in human astrocytomas. *Pathol Oncol Res* 2006;**12**(3):143–7.
8. Thotakura M, Tirumalasetti N, Krishna R. Role of Ki-67 labeling index as an adjunct to the histopathological diagnosis and grading of astrocytomas. *J Cancer Res Ther* 2014;**10**(3):641–5.
9. Chen WJ, He DS, Tang RX, *et al*. Ki-67 is a valuable prognostic factor in gliomas: evidence from a systematic review and meta-analysis. *Asian Pac J Cancer Prev* 2015;**16**(2):411–20.
10. Bell EH, Pugh SL, McElroy JP, *et al*. Molecular-based recursive partitioning analysis model for glioblastoma in the temozolomide era: a correlative analysis based on NRG Oncology RTOG 0525. *JAMA Oncol* 2017;**3**(6):784–92.
11. Liu Z, Wang S, Dong D, *et al*. The applications of radiomics in precision diagnosis and treatment of oncology: opportunities and challenges. *Theranostics* 2019;**9**(5):1303–22.
12. Lambin P, Leijenaar RTH, Deist TM, *et al*. Radiomics: the bridge between medical imaging and personalized medicine. *Nat Rev Clin Oncol* 2017;**14**(12):749–62.
13. Sala E, Mema E, Himoto Y, *et al*. Unravelling tumour heterogeneity using next-generation imaging: radiomics, radiogenomics, and habitat imaging. *Clin Radiol* 2017;**72**(1):3–10.
14. Hwan-Ho C, Hyunjin P. Classification of low-grade and high-grade glioma using multi-modal image radiomics features. *Conf Proc IEEE Eng Med Biol Soc* 2017;**2017**:3081–4.
15. De Looze C, Beausang A, Cryan J, *et al*. Machine learning: a useful radiological adjunct in determination of a newly diagnosed glioma's grade and IDH status. *J Neurooncol* 2018 Sep;**139**(2):491–9.

16. Su C, Jiang J, Zhang S, *et al*. Radiomics based on multicontrast MRI can precisely differentiate among glioma subtypes and predict tumour-proliferative behaviour. *Eur Radiol* 2019 Apr;**29**(4):1986–96.
17. Li Y, Qian Z, Xu K, *et al*. Radiomic features predict Ki-67 expression level and survival in lower grade gliomas. *J Neurooncol* 2017;**135**(2):317–24.
18. Liu Z, Wang Y, Liu X, *et al*. Radiomics analysis allows for precise prediction of epilepsy in patients with low-grade gliomas. *Neuroimage Clin* 2018;**19**:271–8.
19. Kickingereder P, Neuberger U, Bonekamp D, *et al*. Radiomic subtyping improves disease stratification beyond key molecular, clinical, and standard imaging characteristics in patients with glioblastoma. *Neuro Oncol* 2018;**20**(6):848–57.
20. Korfiatis P, Erickson B. Deep learning can see the unseeable: predicting molecular markers from MRI of brain gliomas. *Clin Radiol* 2019;**74**(5):367–73.
21. Kim MM, Parolia A, Dunphy MP, *et al*. Non-invasive metabolic imaging of brain tumours in the era of precision medicine. *Nat Rev Clin Oncol* 2016;**13**(12):725–39.
22. Yoon JH, Kim JH, Kang WJ, *et al*. Grading of cerebral glioma with multiparametric MR imaging and ^{18}F-FDG-PET: concordance and accuracy. *Eur Radiol* 2014;**24**(2):380–9.
23. Dankbaar JW, Snijders TJ, Robe PA, *et al*. The use of ^{18}F-FDG PET to differentiate progressive disease from treatment induced necrosis in high grade glioma. *J Neurooncol* 2015;**125**(1):167–75.
24. Santra A, Kumar R, Sharma P, *et al*. F-18 FDG PET-CT for predicting survival in patients with recurrent glioma: a prospective study. *Neuroradiology* 2011;**53**(12):1017–24.
25. Zhang Y, Xu H, Wang H, *et al*. Fluorine-18-deoxyglucose positron emission tomography/computed tomography with Ki67 and GLUT-1 immunohistochemistry for evaluation of the radiosensitization effect of oleanolic acid on C6 rat gliomas. *Nucl Med Commun* 2015;**36**(1):21–7.
26. Chen W, Cloughesy T, Kamdar N, *et al*. Imaging proliferation in brain tumours with ^{18}F-FLT PET: comparison with 18F-FDG. *J Nucl Med* 2005;**46**(6):945–52.
27. Chicklore S, Goh V, Siddique M, *et al*. Quantifying tumour heterogeneity in ^{18}F-FDG PET/CT imaging by texture analysis. *Eur J Nucl Med Mol Imaging* 2013;**40**(1):133–40.
28. Yip SS, Kim J, Coroller TP, *et al*. Associations between somatic mutations and metabolic imaging phenotypes in non-small cell lung cancer. *J Nucl Med* 2017;**58**(4):569–76.
29. Hatt M, Tixier F, Visvikis D, *et al*. Radiomics in PET/CT: more than meets the eye? *J Nucl Med* 2017;**58**(3):365–6.
30. Ahn HK, Lee H, Kim SG, *et al*. Pre-treatment ^{18}F-FDG PET-based radiomics predict survival in resected non-small cell lung cancer. *Clin Radiol* 2019;**74**(6):467–73.
31. Cai J, Zhang C, Zhang W, *et al*. ATRX, IDH1-R132H and Ki-67 immunohistochemistry as a classification scheme for astrocytic tumours. *Oncoscience* 2016;**3**(7–8):258–65.
32. van Griethuysen JJM, Fedorov A, Parmar C, *et al*. Computational radiomics system to decode the radiographic phenotype. *Cancer Res* 2017;**77**(21):e104–7.
33. Kohavi R, John GH. Wrappers for feature subset selection. *Artif Intell* 1997;**97**(1):273–324.
34. Guyon I, Weston J, Barnhill S, *et al*. Gene selection for cancer classification using support vector machines. *Machine Learn* 2002;**46**(1):389–422.
35. Liu Z, Li Z, Qu J, *et al*. Radiomics of multi-parametric MRI for pretreatment prediction of pathological complete response to neoadjuvant chemotherapy in breast cancer: a multicenter study. *Clin Cancer Res* 2019. clincanres.3190.2018.
36. Bozdogan H. Model selection and Akaike's information criterion (AIC): the general theory and its analytical extensions. *Psychometrika* 1987;**52**(3):345–70.
37. Liu Z, Zhang XY, Shi YJ, *et al*. Radiomics analysis for evaluation of pathological complete response to neoadjuvant chemoradiotherapy in locally advanced rectal cancer. *Clin Cancer Res* 2017;**23**(23):7253–62.
38. Liu C, Zhang H, Pan Y, *et al*. Towards MIB-1 and p53 detection in glioma magnetic resonance image: a novel computational image analysis method. *Phys Med Biol* 2012;**57**(24):8393–404.
39. Alexiou GA, Zikou A, Tsiouris S, *et al*. Correlation of diffusion tensor, dynamic susceptibility contrast MRI and (99m)Tc-Tetrofosmin brain SPECT with tumour grade and Ki-67 immunohistochemistry in glioma. *Clin Neurol Neurosurg* 2014;**116**:41–5.
40. Fudaba H, Shimomura T, Abe T, *et al*. Comparison of multiple parameters obtained on 3T pulsed arterial spin-labeling, diffusion tensor imaging, and MRS and the Ki-67 labeling index in evaluating glioma grading. *AJNR Am J Neuroradiol* 2014;**35**(11):2091–8.
41. Nielsen LAG, Bangso JA, Lindahl KH, *et al*. Evaluation of the proliferation marker Ki-67 in gliomas: interobserver variability and digital quantification. *Diagn Pathol* 2018;**13**(1):38.
42. Warburg O. The metabolism of carcinoma cells. *J Cancer Res* 1925;**9**(1):148–63.
43. Racker E. Bioenergetics and the problem of tumour growth: an understanding of the mechanism of the generation and control of biological energy may shed light on the problem of tumour growth. *Am Sci* 1972;**60**:56–63.
44. Maher EA, Marin-Valencia I, Bachoo RM, *et al*. Metabolism of [U–^{13}C] glucose in human brain tumours *in vivo*. *NMR Biomed* 2012;**25**(11):1234–44.
45. Deng SM, Zhang W, Zhang B, *et al*. Correlation between the uptake of ^{18}F-fluorodeoxyglucose (^{18}F-FDG) and the expression of proliferation-associated antigen Ki-67 in cancer patients: a meta-analysis. *PLoS One* 2015;**10**(6):e0129028.
46. Price SJ, Fryer TD, Cleij MC, *et al*. Imaging regional variation of cellular proliferation in gliomas using 3'-deoxy-3'-[^{18}F]fluorothymidine positron-emission tomography: an image-guided biopsy study. *Clin Radiol* 2009;**64**(1):52–63.